Click Here for Full Article

Interpretation of tropical thermocline cooling in the Indian and Pacific oceans during recent decades

Weiqing Han,[1] Gerald A. Meehl,[2] and Aixue Hu[2]

[1] A warming trend has been detected in the world's oceans in recent decades. The basin-averaged warming, however, shows a complex vertical structure in the Indian and Pacific oceans. Warming in the upper ocean-with maxima near the surface- accompanies a strong cooling in the upper thermocline. Analysis of observed data and model solutions from this study reveals that the complex structure is confined mainly to the tropics. While increased greenhouse gases act to warm up the upper ocean by increasing downward surface heat fluxes, anomalous winds in the tropics cause upward Ekman pumping velocity and shoal the thermocline, resulting in an upper-thermocline cooling. This cooling process is well demonstrated by a simple model based on the ventilated thermocline theory. The study has important implications for climate change and fisheries. **Citation:** Han, W., G. A. Meehl, and A. Hu (2006), Interpretation of tropical thermocline cooling in the Indian and Pacific oceans during recent decades, *Geophys. Res. Lett.*, *33*, L23615, doi:10.1029/2006GL027982.

1. Introduction

[2] Warming of global oceans in recent decades has been detected by a wide-range of observations [e.g., *Intergovernmental Panel on Climate Change*, 2001; *Levitus et al.*, 2001, 2005]. This warming signal has been attributed mostly to human-induced greenhouse gases, which increase surface heat fluxes into the ocean [*Levitus et al.*, 2001, 2005; *Barnett et al.*, 2001, 2005; *Hansen et al.*, 2002; *Reichert et al.*, 2002; *Gent and Danabasoglu*, 2004; *Gregory et al.*, 2004]. Recently, *Barnett et al.* [2005] and *Pierce et al.* [2006] examined how the surface warming signals penetrate down into deeper oceans. They showed that the warming has a distinct vertical structure in the Indian and Pacific oceans, with large amplitude warming above ~100 m, cooling near 100–250 m, and a weaker warming around 250–700 m. Signals associated with this structure significantly exceed data uncertainties [*Barnett et al.*, 2005; *Pierce et al.*, 2006]. The structure discussed above, however, was based on the temperature data averaged over an entire basin for each ocean. It is not clear whether this structure occurs throughout the basin or if it is confined to a specific latitudinal band. It is not known how and why the upper-thermocline cooling was caused.

[3] Here we focus on investigating the role of tropical winds in causing the thermocline cooling in the Indian and Pacific oceans since 1960. This study will not only contribute to our understanding of climate variability and change, but also could benefit fish industry because changes in vertical structure of oceanic temperature can have substantial effects on marine ecosystems and fisheries (e.g., a review paper by *Brill* [1994]).

2. Data and Models

[4] We use a recently upgraded observed ocean data set of *Levitus et al.* [2005], which provides the best available description of the ocean's temperature structure and its evolution with time. We also analyze the latest version of data from Simple Ocean Data Assimilation in Parallel Ocean Program (SODA-POP) (J. Carton and B. Giese, A reanalysis of ocean climate using SODA, submitted to *Monthly Weather Review*, 2006), together with the European Centre for Medium-Range Weather Forecasting (ECMWF) 40-year reanalysis (ERA40) winds that are used to force the SODA-POP model. A two-layer model of the ventilated thermocline and a linear, two-layer model based on equatorial beta-plane approximation are utilized to understand the dynamics of the upper-thermocline cooling. Our period of interest is 1960–1999, when all data described above are available.

3. Results

[5] Figure 1 shows meridional sections of observed temperature anomalies in the upper 1000 m in the Indian and Pacific oceans, based on the zonal-mean temperature difference between 1990s and 1960s for each basin (Figures 1a and 1b). In both oceans, there is strong cooling in the upper thermocline that accompanies significant warming near the surface and weak warming in the lower thermolcine. This complex structure is primarily confined to the tropics. Linear trends of temperature for the same period of time (not shown) bear a remarkable resemblance to Figures 1a and 1b. These structures are reasonably reproduced by the SODA-POP data in the tropical basins (Figures 1c and 1d), although there are some quantitative differences. The largest disparities between the two datasets occur in the southern oceans south of 35°S, where the observations are sparse. In the tropics, our region of interest, the observations and SODA-POP data agree reasonably well. The anomalous temperature structures in the two oceans bear many similarities. There are, however, significant differences. Below, we discuss each ocean separately.

[6] In the Indian Ocean, cooling of the thermocline is mainly observed at 17°S–5°N (Figure 1a), with the maxi-

---

[1]Department of Atmospheric and Oceanic Sciences, University of Colorado, Boulder, Colorado, USA.
[2]Climate and Global Dynamics Division, National Center for Atmospheric Research, Boulder, Colorado, USA.
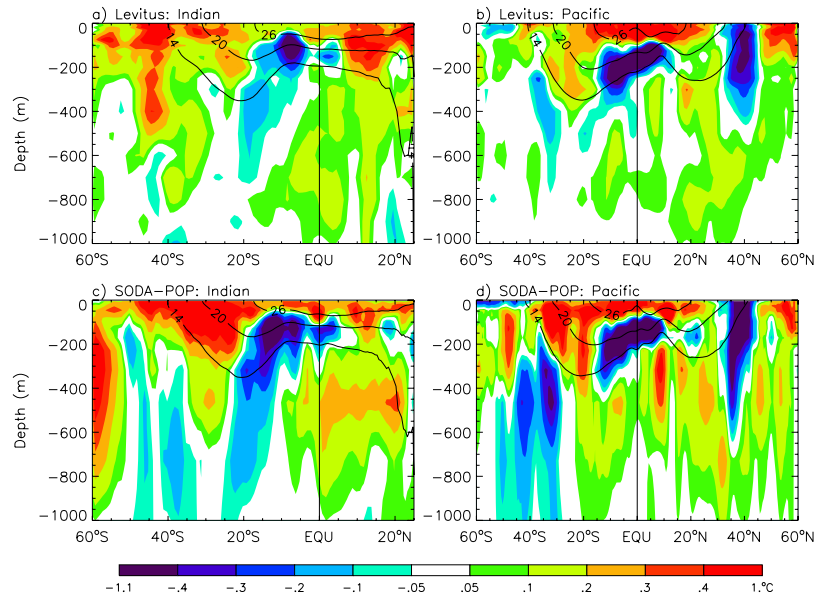
Figure 1. Meridional sections of temperature anomalies (in °C) for the upper 1000 m of the Indian and Pacific oceans, based on zonally averaged temperature difference between 1990s and 1960s for each basin. (a and b) Levitus pentad (5-year mean) data; (c and d) SODA-POP monthly data. The 14°C, 20°C and 26°C isotherms for 1960s are also plotted in each panel.

mum upper-thermocline cooling occurring south of the equator near $10°S-3°S$, which is the strongest upwelling zone over the tropical Indian Ocean [*McCreary et al.*, 1993; *Murtugudde et al.*, 1999; *Xie et al.* 2002]. In this region, wind stress curl associated with the Asian monsoon causes a positive (upward) Ekman pumping velocity, w_e (dark solid and dark dashed curves of Figure 2), which shoals the thermocline and produces a thermocline dome (Figure 3a) [*Xie et al.*, 2002]. The latitudinal distributions of w_e shown in Figure 2 (top), which is calculated from the ERA40 winds, are consistent with the w_e distributions shown by *Pedlosky* [1998, Figure 2.2.3] for both the Indian and Pacific oceans. In the above, $w_e = \frac{\partial}{\partial x}\left(\frac{\tau^y}{\rho_0 f}\right) - \frac{\partial}{\partial y}\left(\frac{\tau^x}{\rho_0 f}\right)$, where $\rho_0 = 1$ g cm^{-3} is the mean density of sea water, f is Coriolis parameter, and (τ^x, τ^y) are the zonal and meridional wind stress.

[7] Interestingly, the upward w_e at $10°S-3°S$ is enhanced and downward (negative) w_e at $17°S-10°S$ is weakened during 1990s (dark dashed) relative to 1960s (dark solid), which act to shoal the thermocline (Figures 2, bottom) and produce a thermocline cooling (Figure 3a). The strongest cooling occurs near the thermocline dome where vertical temperature gradient is strongest (Figures 1a, 1c, and 3a); thus a small vertical displacement of thermocline can cause a large temperature change. Near the equator ($3°S-5°N$), thermocline cooling is weaker (Figure 1a), which coincides with equatorial westerly wind anomalies (Figure 2, bottom). In fact, at ($2°N-5°N$), the positive w_e is also enhanced during 1990s, which coincides with the shallower thermocline and cooling there (Figures 1a and 2). Note that the shallow thermocline signals on both sides of the equator are connected near the western boundary (Figure 2, bottom), suggesting the off-equatorial influence on the equator. For example, signals of the off-equatorial shoaling thermocline can propagate westward via Rossby waves to the western boundary, where they propagate equatorward as coastal

Kelvin waves and subsequently propagate eastward as equatorial Kelvin waves.

[8] In the Pacific, strong cooling of the thermocline together with a near surface warming occurs from $15°S$ to $10°N$ across the equator (Figures 1b and 1d). Within this latitudinal band, w_e is negative during both 1960s and 1990s in the off-equatorial regions, except for the intertropical
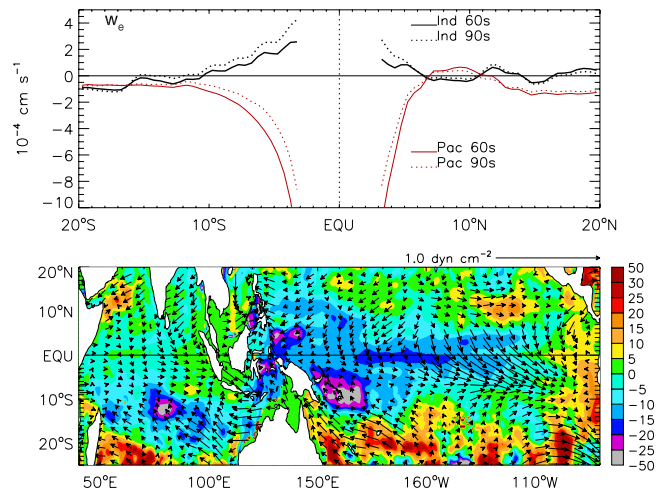

Figure 2. (top) Ekman pumping velocity (w_e) zonally averaged over the Indian ocean for 1960s (dark solid) and 1990s (dark dashed), and over the Pacific for 1960s (red solid) and 1990s (red dashed). Near the equator, w_e is undefined and thus is not shown. The ERA40 winds, the forcing fields of the SODA-POP model, are used to calculate w_e. Units: 10^{-4} cm s^{-1}. (bottom) Differences of the 20°C isotherm depth (in m) between 1990s and 1960s. Arrows are the wind stress differences (in dyn cm^{-2}) between 1990s and 1960s.
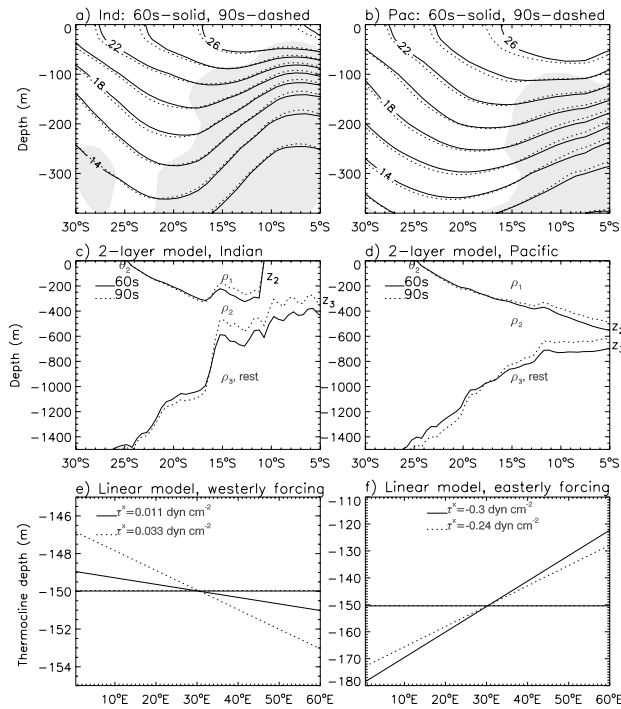
Figure 3. (a) Zonally averaged isotherms during 1960s (solid) and 1990s (dashed) for the Indian Ocean based on the Levitus pentad data. Cooling regions are shaded gray. Units: °C. (b) Same as Figure 3a except for the Pacific. (c) The two-layer model of the ventilated thermocline. Layers 1 and 2 are in motion. Layer 3 is assumed to be at rest. The interface between layer 2 and layer 1 rises to meet the mixed layer at $\theta_2 = 25°$S where $f = f_2$. Depths for layers 1 and 2 are z_2 and z_3 (in m), which are forced by ERA40 winds of 1960s (solid) and 1990s (dashed). To obtain D_0^2 in z_3 equation, we use the zonal mean w_e and choose the basin width of $\phi_e - \phi = 25°$, which is located west of the shadow zone in the region south of 11°S (figure for shadow zone not shown). Between 11°S and 5°S, w_e is upward and layer 1 outcrops at 11°S where $w_e = 0$. In this region, only layer 2 exists and it is directly forced by w_e. Density values of ρ_1, ρ_2 and ρ_3 are obtained by averaging Levitus density over 30°S–25°N of the Indian Ocean above 100 m, from 100 m to 550 m, and below 550 m, respectively, during 1960s. (d) Same as Figure 3c except for the Pacific Ocean. The basin width $\phi_e - \phi = 25°$ ensures that longitude ϕ is located west of the shadow zone (not shown). Layer densities are averaged over 30°S–30°N of the Pacific during 1960s; (e) Depth of the upper thermocline (in m) from a linear, 2-layer reduced gravity model based on equatorial beta-plane approximation in a rectangular basin of 0–60°E and 30°S–30°N. The model includes Laplacian horizontal mixing and vertical diffusion. The tilted solid (dashed) line is the thermocline depth forced by a uniform westerly wind with $\tau^x = 0.011$ dyn cm^{-2} ($\tau^x = 0.033$ dyn cm^{-2}), the 5°S–5°N mean of ERA40 τ^x in the Indian Ocean during 1960s (1990s). The horizontal solid and dashed lines are the zonal mean of the thermocline depths. The solutions shown here is from the model year 11. (f) Same as Figure 3e except for easterly wind forcing during 1960s (solid) and 1990s (dashed) of ERA40 winds averaged over the equatorial Pacific. The easterly trade weakens by about 20% during 1990s relative to 1960s.

convergence zone (ITCZ) near 9°N where w_e is positive (Figure 2, red curves). The downward Ekman pumping velocity during 1990s is weaker than that of 1960s from 15°S to 6°N, which coincides with most region of the observed thermocline cooling. This suggests that the reduced downward w_e may act to shoal the thermocline (Figures 2 and 3b) and thus contribute to the cooling. The shallow thermocline signals off the equator can affect the equatorial region via Rossby waves, coastal and equatorial Kelvin waves. Near the equator, westerly wind anomalies during 1990s weaken the easterly trades, reduce the east-west thermocline slope, shoal the thermocline in the west and deepen it in the east (Figure 2, bottom).

[9] To confirm our above analysis, we use a two-layer model of ventilated thermocline based on the quasi-geostrophic theory in the off-equatorial region (Figures 3c and 3d) [*Luyten et al.*, 1983; *Pedlosky*, 1998]. The motivation and scientific basis for applying the ventilated thermocline theory are that the observed cooling occurs mainly in the tropical thermocline region, and the time scale for the cooling is a few decades which is long enough to ensure the validity of the steady state solution of the ventilated thermocline.

[10] Below we briefly describe the 2-layer model. For details, see *Pedlosky* [1998, section 4.4]. In the two-layer region (equatorward of θ_2 in Figure 3d), solutions for the depths of layers 2 and 1 are:

$$z_3 = -\sqrt{\frac{D_0^2 + Z_3^2}{1 + \frac{\gamma_1}{\gamma_2}\left(1 - \frac{f}{f_2}\right)^2}}, \quad z_2 = \left(1 - \frac{f}{f_2}\right)z_3, \qquad (1)$$

where $D_0^2 (\phi, \theta) = -\frac{2f^2}{\beta\gamma_2}\int_\phi^{\phi_e} w_e(\phi', \theta)R\cos\theta d\phi'$. In the above $\gamma_1 = \frac{\rho_2 - \rho_1}{\rho}$, $\gamma_2 = \frac{\rho_3 - \rho_2}{\rho}$, ρ_1, ρ_2, and ρ_3 are the densities of layer 1, layer 2, and deep ocean that is quiescent, ρ is the mean density of an individual ocean, Z_3 is the eastern boundary value of z_3 and it is chosen as 550 m, R is the earth's radius, ϕ is longitude, ϕ_e is the longitude at the eastern boundary, θ is latitude, and f_2 is the Coriolis parameter at latitude θ_2 where the interface between layer 2 and layer 1 rises to meet the mixed layer. We choose $\theta_2 = 25°$S, and ρ_1, ρ_2, and ρ_3 the averaged Levitus densities in layers above 100 m, 100~550 m, and below 550 m for each ocean during 1960s in our calculations for Figures 3c and 3d. In the single layer region (poleward of ϕ_2 in Figures 3c and 3d), the solution is in Sverdrup balance:

$$z_3 = -\sqrt{D_0^2 + Z_3^2}. \qquad (2)$$

[11] One exception is for the Indian Ocean equatorward of 11°S region, where w_e is positive (Figure 2, top) and layer 1 outcrops (Figure 3c). This region is in the shadow zone, and only layer 2 exists. Its depth is determined by equation (2), which is in Sverdrup balance.

[12] The above equations demonstrate that layer depths z_3 and z_2 vary with D_0^2, which is determined by zonal integral of Ekman pumping velocity w_e. When w_e changes, z_3 and z_2 change and thus cause isotherms to move up and down.

[13] In the Indian Ocean, the positive w_e anomaly during 1990s moves the thermocline upward (compare the dashed

and solid curves of Figure 3c). This upward shift mimics the observed shoaling of the thermocline (Figure 3a), producing an anomalous thermocline cooling. The calculation is only performed in the southern hemisphere, because subduction mainly occurs in the southern subtropical Indian Ocean where the subducted water flows to the tropical thermocline. The Arabian Sea subduction and the Indonesian Throughflow complicate the situation [*Schott et al.*, 2004], but examination of these aspects is beyond the scope of this paper. Note that the decadal-mean patterns shown here represent steady states, which are reached by radiating transient waves. As mentioned earlier, the shoaling thermocline shown in Figure 3c can propagate westward as Rossby waves. When they arrive at the western boundary, the signals can propagate equatorward as coastal Kelvin waves and subsequently eastward as equatorial Kelvin waves, causing a shallow thermocline in the equatorial region in the decadal mean patterns.

[14] In the Pacific, the positive w_e anomaly during 1990s reduces the downward Ekman pumping velocity (red curves in Figure 2) and thus shoals the thermocline (Figure 3d). As for the Indian Ocean, this upward shift of thermocline resembles the observed thermocline shoaling (compare Figures 3d and 3b), demonstrating the important role played by the tropical winds in causing the thermocline cooling. Similar model solutions are found for the north Pacific. We obtain an upward shift of the thermocline in the shadow zone near $5°N–7°N$, where thermocline cooling is also observed. In this region, layer 2 has no motion and all the Sverdrup transport is carried by layer 1. These shallow thermocline signals can affect the equatorial region via Rossby and Kelvin waves. *Vivier et al.* [1999] suggested the importance of wave processes and wind stress curl on the sea level variations in the Pacific Ocean, although their focus is on seasonal-to-interannual timescales.

[15] In the equatorial region where quasi-geostrophic approximation is not valid, zonal wind anomalies during 1990s are westerlies in both oceans (Figure 2, bottom), which represent weakened easterly trades in the Pacific and enhanced westerlies in the Indian Ocean relative to 1960s. Experiments using a linear, 2-layer reduced gravity model with horizontal and vertical mixing suggest that a weakened (enhanced) equatorial easterly (westerly) in the Pacific (Indian Ocean) reduces (strengthens) the east-west thermocline slope (Figures 3e and 3f), as suggested by *McPhaden and Zhang* [2002]. This dynamical adjustment, however, does not induce net changes in the zonal-mean thermocline depth in the steady solution of the linear model that excludes surface heating process (Figures 3e and 3f, horizontal lines). By considering surface heating, a relaxation of easterly trade in the Pacific may contribute to the net thermocline shoaling, because a deepened thermocline in the eastern basin due to the relaxation of the easterlies reduces upwelling, increases SST, and thus decreases surface turbulent heat fluxes into the ocean [*Boccaletti et al.*, 2004]. In the Indian Ocean, this scenario may not hold, because thermocline is generally deep (>110 m) across the equatorial basin (not shown) and a further deepened thermocline may not cause appreciable SST changes.

[16] Because the upper ocean has warmed up in the past few decades, the stratification of each ocean has changed. To estimate this effect, we find a new set of solutions to the 2-layer model of ventilated thermocline for each ocean using the density structure of 1990s instead of 1960s. Our results show that under the stratification of 1990s, the system adjusts to a new equilibrium state in which the thermocline is shallower in most region of the tropical basins for both oceans where thermocline cooling is observed (not shown). This effect, however, is less than 10% of the thermocline change caused by the anomalous winds.

4. Summary and Discussion

[17] The observed complex vertical warming structure in the Indian and Pacific oceans [*Barnett et al.*, 2005] is primarily confined to the tropics. While the human-induced greenhouse gases tend to heat up the oceanic surface, the warming signal in the subtropics can penetrate downward through subtropical subduction and be advected to the tropics (Figure 1) [*Gu and Philander*, 1997] by the shallow, meridional overturning circulation in the upper ocean, which is often referred to as the subtropical cell (STC; [*McCreary and Lu*, 1994; *Liu*, 1994; *Liu et al.*, 1994; *Kleeman et al.*, 1999; *Solomon et al.*, 2003; *Schott et al.*, 2004; *Barnett et al.*, 2005]).

[18] Using a simple, 2-layer model of the ventilated thermocline and a linear, 2-layer reduced gravity model for the equatorial ocean, we demonstrate that the observed upper-thermocline cooling in both oceans results primarily from the anomalous, upward Ekman pumping velocity (w_e) in the tropics, which moves the thermocline upward and produces a cooling in the thermocline. The shallow thermocline signals in the off-equatorial regions can cause a shoaling thermocline at the equator via westward propagating Rossby waves, coastal Kelvin waves near the western boundary, and equatorial Kelvin waves. Relaxation of the easterly trade may also contribute to the thermocline shoaling in the equatorial Pacific, as suggested by *Boccaletti et al.* [2004]. This cooling effect overcomes the warming discussed above in the upper-thermocline region, where vertical gradients of temperature are large. Thus a small vertical displacement of thermocline can cause a large temperature change. The changes of oceanic stratification from 1960s to 1990s also contribute to the observed shoaling thermocline, but its amplitudes are less than 10% of those caused by anomalous winds.

[19] The simple models used here are meant to illustrate the major wind-driven processes that may cause the thermocline cooling. For an accurate simulation of the thermocline cooling, they have limitations. For example, the ventilated thermocline model assumes a known eastern boundary situation, and it excludes the effects of mixing and anomalous heat advection that can also affect the temperature of the thermocline. Nevertheless, it isolates the major wind-driven processes and is a useful tool for understanding the changes of the thermocline. In addition to winds, some other extratropical processes have also been suggested to be able to influence the depth of tropical thermocline. *Huang and Pedlosky* [2000] suggested that warming in extratropics can cause an upward movement of the tropical thermocline. *Boccaletti et al.* [2004] argued that warming (or decrease in heat loss) in higher latitudes can result in a deepened tropical thermocline. It has been

suggested that strengths of the STCs in the Pacific have been weakening from 1960s to 1990s [e.g., *McPhaden and Zhang*, 2002; *Capotondi et al.*, 2005], but they begin to enhance in the past few years [*McPhaden and Zhang*, 2004]. The weakened STCs reduce the transport of colder subtropical water into, and warmer tropical water out of, the tropics, which can affect the tropical thermocline. In the Indian Ocean, slowing down of the cross equatorial cell for the period of interest is also indicated [*Schoenefeldt and Schott*, 2006]. A weakening of the southern STC is suggested only for late 1990s relative to early 1990s [*Lee*, 2004]. Quantitative examinations of the extratropical influence and effects of the STC transports are beyond the scope of this paper, but are an essential part for our ongoing research.

[20] Since the upper ocean warming in the past few decades has been attributed mostly to anthropogenic forcing by existing studies (section 1), changes of oceanic stratification are likely related to human effects. Is the anthropogenic forcing the possible cause for the anomalous winds? This is an interesting topic for our future investigation.

References

Barnett, T. P., D. W. Pierce, and R. Schnur (2001), Detection of anthropogenic climate change in the world's oceans, *Science*, 292, 270–274.

Barnett, T. P., et al. (2005), Penetration of human-induced warming into the world's oceans, *Science*, 309, 284–287.

Brill, R. W. (1994), A review of temperature and oxygen tolerance studies of tunas pertinent to fisheries oceanography, movement models and stock assessments, *Fish Oceanogr.*, 3, 204–216.

Boccaletti, G., R. C. Pacanowski, S. G. H. Philander, and A. V. Fedorov (2004), The thermal structure of the upper ocean, *J. Phys. Oceanogr.*, 34, 888–902.

Capotondi, A., M. A. Alexander, C. Deser, and M. J. McPhaden (2005), Anatomy and decadal evolution of the Pacific subtropical-tropical cells (STCs), *J. Clim.*, 18, 3739–3758.

Gent, P. R., and G. Danabasoglu (2004), Heat uptake and the thermohaline circulation in the Community Climate System Model, version 2, *J. Clim.*, 17, 4058–4069.

Gregory, J. M., H. T. Banks, P. A. Stott, J. A. Lowe, and M. D. Palmer (2004), Simulated and observed decadal variability in ocean heat content, *Geophys. Res. Lett.*, 31, L15312, doi:10.1029/2004GL020258.

Gu, D., and S. G. H. Philander (1997), Interdecadal climate fluctuations that depend on exchanges between the tropics and extratropics, *Science*, 275, 805–807.

Hansen, J., et al. (2002), Climate forcings in Goddard Institute for Space Studies SI2000 simulations, *J. Geophys. Res.*, 107(D18), 4347, doi:10.1029/2001JD001143.

Huang, R. X., and J. Pedlosky (2000), Climate variability of the equatorial thermocline inferred from a two-moving-layer model of the ventilated thermocline, *J. Phys. Oceanogr.*, 30, 2610–2626.

Intergovernmental Panel on Climate Change (2001), *Climate Change 2001: Synthesis Report*, 397 pp., Cambridge Univ. Press, New York.

Kleeman, R., J. P. McCreary, and B. Klinger (1999), A mechanism for generating ENSO decadal variability, *Geophys. Res. Lett.*, 26, 1743–1746.

Lee, T. (2004), Decadal weakening of the shallow overturning circulation in the South Indian Ocean, *Geophys. Res. Lett.*, 31, L18305, doi:10.1029/2004GL020884.

Levitus, S., J. I. Antonov, J. Wang, T. L. Delworth, K. W. Dixon, and A. J. Broccoli (2001), Anthropogenic warming of Earth's climate system, *Science*, 292, 267–270.

Levitus, S., J. Antonov, and T. Boyer (2005), Warming of the world ocean, 1955–2003, *Geophys. Res. Lett.*, 32, L02604, doi:10.1029/2004GL021592.

Liu, Z. (1994), A simple model of the mass exchange between the subtropical and tropical ocean, *J. Phys. Oceanogr.*, 24, 1153–1165.

Liu, Z., S. G. H. Philander, and R. C. Pacanowski (1994), A GCM study of the tropical-subtropical upper-ocean exchange, *J. Phys. Oceanogr.*, 24, 2606–2623.

Luyten, J. R., J. Pedlosky, and H. Stommel (1983), The ventilated thermocline, *J. Phys. Oceanogr.*, 13, 292–309.

McCreary, J. P., and P. Lu (1994), Interaction between the subtropical and equatorial ocean circulations: The subtropical cell, *J. Phys. Oceanogr.*, 24, 466–497.

McCreary, J. P., P. K. Kundu, and R. L. Molinari (1993), A numerical investigation of dynamics, thermodynamics, and mixed-layer processes in the Indian Ocean, *Prog. Oceanogr.*, 31, 181–224.

McPhaden, M. J., and D. Zhang (2002), Slowdown of the meridional overturning circulation in the upper Pacific Ocean, *Nature*, 415, 603–608.

McPhaden, M. J., and D. Zhang (2004), Pacific Ocean circulation rebounds, *Geophys. Res. Lett.*, 31, L18301, doi:10.1029/2004GL020727.

Murtugudde, R., S. R. Signorini, J. R. Christian, A. J. Busalacchi, C. R. McClain, and J. Picaut (1999), Ocean color variability of the tropical Indo-Pacific basin observed by SeaWiFS during 1997–1998, *J. Geophys. Res.*, 104, 18,351–18,366.

Pedlosky, J. (1998), *Ocean Circulation Theory*, 453 pp., Springer, New York.

Pierce, D. W., et al. (2006), Anthropogenic warming of the oceans: Observations and model results, *J. Clim.*, 19, 1873–1900.

Reichert, B. K., R. Schnur, and L. Bengtsson (2002), Global ocean warming tied to anthropogenic forcing, *Geophys. Res. Lett.*, 29(11), 1525, doi:10.1029/2001GL013954.

Schoenefeldt, R., and F. Schott (2006), Decadal variability of the Indian Ocean cross-equatorial exchange in SODA, *Geophys. Res. Lett.*, 33, L08602, doi:10.1029/2006GL025891.

Schott, F., J. P. McCreary, and G. C. Johnson (2004), Shallow overturning circulations of the tropical-subtropical oceans, in *Earth's Climate: The Ocean–Atmosphere Interaction, Geophys. Monogr. Ser.*, vol. 147, edited by C. Wang, S.-P. Xie, J. A. Carton, pp. 261–304, AGU, Washington, D. C.

Solomon, A., et al. (2003), Interannual and decadal variability in an intermediate coupled model of the Pacific region, *J. Clim.*, 16, 383–405.

Vivier, F., K. A. Kelly, and L. Thompson (1999), Contributions of wind forcing, waves, and surface heating to sea surface height observations in the Pacific Ocean, *J. Geophys. Res.*, 104, 20,767–20,788.

Xie, S.-P., H. Annamalai, F. A. Schott, and J. P. McCreary (2002), Structure and mechanisms of south Indian Ocean climate variability, *J. Clim.*, 15, 864–878.

———————————

W. Han, Department of Atmospheric and Oceanic Sciences, University of Colorado, UCB 311, Boulder, CO 80309, USA. (whan@enso.colorado.edu)

A. Hu and G. A. Meehl, Climate and Global Dynamics Division, National Center for Atmospheric Research, PO Box 3000, Boulder, CO 80305, USA.